Multiple Model Iterative Learning Control of FES Electrode Arrays

Lucy Hodgins [a], Chris T. Freeman [b] and Zehor Belkhatir [c]
School of Electronics and Computer Science, University of Southampton, Southampton, UK
{lgh1g19, ctf1, z.belkhatir}@soton.ac.uk

Keywords: Iterative Learning Control, Functional Electrical Stimulation, Multiple Model Switched Adaptive Control, Stroke Rehabilitation

Abstract: Stroke is a common cause of hand and upper limb disability, but current rehabilitation approaches do not adequately support successful recovery. Functional electrical stimulation (FES) is the most widely used assistive technology, and is able to support accurate hand and wrist motion when applied using multi-element electrode arrays. However, accurate movements have only been possible using an iterative learning control (ILC) approach involving many repeated model identification tests. This lengthy process limits wide-spread use. This paper presents a solution for FES electrode array control using estimation-based multiple-model ILC (EMMILC), in which a set of parameterised models is used to automatically update the stimulation applied to each array element every time a task is carried out. This removes the need for model identification, significantly improving system usability whilst maintaining high performance. Experimental results demonstrate that EMMILC reduces the average number of tests from 16 to 3, compared to the most accurate existing approach.

1 INTRODUCTION

Stroke is a leading cause of disability worldwide, with over 12 million new cases each year (Feigin et al., 2022). Approximately half of suffers are left with some form of hand or upper limb impairment, which significantly impacts their quality of life (Persson et al., 2012). Movement can be regained through continued repetitive practice of functional tasks, which strengthens neural connections in the brain (Hebbian learning (Hebb, 1949)). However, the level of support provided by conventional physiotherapy is typically inadequate (Stockley et al., 2019), and 62% of people with severe impairment fail to regain dexterous hand motion within six months (Kwakkel et al., 2003).

This motivates the use of assistive technologies, the most common of which is functional electrical stimulation (FES) (Hughes et al., 2014), in which nerves are stimulated via surface electrodes to artificially contract the underlying muscles. Hand movement requires the coordinated motion of a large number of different muscles, which makes FES control challenging. In recent years electrode arrays have enabled more selective stimulation of hand and wrist muscles (Schill et al., 2009; Salchow et al., 2016; ODwyer et al., 2006), with the best results arising through use of iterative learning control (ILC) (Freeman, 2014; Sun and Freeman, 2024). ILC utilises the repetitive nature of rehabilitation to improve performance by updating the control signal using data from previous attempts. However, existing ILC approaches require lengthy identification procedures, meaning they have not yet translated into clinical practice.

The need for model identification can be mitigated by fusing ILC with adaptive control. One adaptive approach that has previously shown promise in the context of FES is multiple model switched adaptive control (MMSAC) (Brend et al., 2015), in which a set of controllers are designed based on a set of system models that capture the presumed uncertainty. The framework determines which plant most closely fits the system behaviour at a given point in time, before switching the corresponding controller into the closed-loop. The MMSAC framework was adapted for use with ILC in (Freeman and French, 2015) to create a framework termed estimation-based multiple model ILC (EMMILC).

This work extends the EMMILC architecture for use with a general class of non-linear systems. This involves defining a principled design framework for specification of the plant model set and controller properties, together with a computationally efficient estimator structure to determine the controller switch-

[a] https://orcid.org/0000-0001-6109-0546
[b] https://orcid.org/0000-0003-0305-9246
[c] https://orcid.org/0000-0001-7277-3895

ing. The EMMILC framework is then applied to control hand and wrist motion using an FES electrode array. Experimental results compare it with the best existing approach, and confirm its practical efficacy.

This paper is structured as follows. Section 2 introduces the necessary background, including a comprehensive model of the hand and wrist stimulated by an FES array, and an overview of ILC. The nonlinear EMMILC framework is developed in Section 3, and Section 4 applies it to FES array based hand and wrist control. Experimental results are then presented in Section 5 before Section 6 concludes the paper.

2 PROBLEM DESCRIPTION AND PRELIMINARIES

FES electrode arrays are composed of n separate electrodes pads, that are arranged in fixed pattern. They are typically printed on polycarbonate and have a hydrogel layer that is placed on the surface of the skin. An FES sequence $u(t) \in \mathbb{R}^n$ is applied to these electrodes over time instances $t = 0,1,...,N$, and the aim is to precisely assist the patient's movement. This is done by selecting a set of q clinically-relevant joint angles $y(t) \in \mathbb{R}^q$ and requiring they track a predefined reference signal trajectory $y_d(t) \in \mathbb{R}^q$.

Since stroke rehabilitation requires repeated task practice, each attempt or 'iteration' of a task is denoted by introducing an additional argument, with variable $k = 1,2,....$ The control aim is to compute input $u(k,t)$ such that the error $e(k,t) = y_d(t) - y(k,t)$ decreases with each sucessive iteration, i.e.

$$\lim_{k\to\infty} e(k,t) = 0, \quad t = 0,1,...,N-1. \tag{1}$$

2.1 Hand and Wrist Structure

The dynamics of the electrically stimulated hand and wrist consists of four key components: the electrode array, the muscle dynamics, the non-linear tendon network, and the rigid body dynamics. Their connection is shown in Figure 1, denoted using operator G^*.

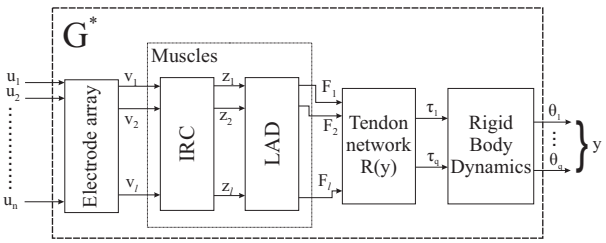

Figure 1: Hand and wrist model structural components.

The stimulation experienced by the ith muscle can be modelled as a linear combination of the FES applied to each element of the n channel electrode array. The stimulation signal $v(k,t) \in \mathbb{R}^l$ experienced by the l underlying muscles therefore has elements

$$v_i(k,t) = \sum_{j=1}^{n} a_{i,j} u_j(k,t), \quad i = 1,...,l \tag{2}$$

where $a_{i,j} \in \mathbb{R}_+$ is the contribution of the jth array element to the ith muscle (Freeman et al., 2016).

The dynamics of the ith muscle can be accurately modelled by a Hammerstein structure, comprising a static function $h_{IRC,i}(v_i(k,t))$ which models the isometric recruitment curve (IRC), cascaded with linear activation dynamics (LAD) (Le et al., 2010). The latter are denoted by the state-space triple $\{M_{A,i}, M_{B,i}, M_{C,i}\}$ with state $\tilde{x}_i(k,t)$. The generated force $F_i(k,t)$ then feeds into a tendon network which generates a moment about each joint angle. The moment arm of the ith muscle about the pth joint is computed using $\frac{dE_i(y_p)}{dy_p}$ where continuous function E is the associated tendon excursion (Feldman and Latash, 2005). Therefore the overall moment vector generated by stimulating all muscles is $\tau(k,t) = R(y(k,t))F(k,t)$ where the (p,i)th element of moment arm matrix $R(y(k,t)) \in \mathbb{R}^{q\times l}$ is $\frac{dE_i(y_p)}{dy_p}(k,t)$.

The moment vector actuates the passive rigid body dynamics of the system which take the general form

$$\begin{aligned} M(y(k,t))\ddot{y}(k,t) + C(y(k,t),\dot{y}(k,t)) + G(y(k,t)) \\ + K(y(k,t),\dot{y}(k,t)) = \tau(k,t) \end{aligned} \tag{3}$$

where $M(\cdot)$ denotes the inertia matrix, $C(\cdot,\cdot)$ is the Coriolis matrix, $G(\cdot)$ the gravity vector, and $K(\cdot,\cdot)$ captures joint stiffness, damping and friction effects.

Combining the above four components yields the overall dynamic system

$$\begin{aligned} \frac{dx(k,t)}{dt} = &\begin{bmatrix} x_2(k,t) \\ M(x_1(k,t))^{-1}X(x(k,t)) \\ M_{A,1}\tilde{x}_1(k,t) \\ \vdots \\ M_{A,l}\tilde{x}_l(k,t) \end{bmatrix} \\ &+ \begin{bmatrix} 0 \\ 0 \\ M_{B,1}h_{IRC,1}(\bar{a}_1 u(k,t)) \\ \vdots \\ M_{B,l}h_{IRC,l}(\bar{a}_l u(k,t)) \end{bmatrix}, \end{aligned} \tag{4}$$

$$y(k,t) = \begin{bmatrix} I & 0 & \dots & 0 \end{bmatrix} x(k,t) := h(x(k,t)), \tag{5}$$

where state vector $x(k,t) = [x_1(k,t)^\top, x_2(k,t)^\top, \tilde{x}_1(k,t)^\top, \cdots, \tilde{x}_l(k,t)^\top]^\top$ and output $y(k,t) = [\theta_1(k,t),...,\theta_q(k,t)]^\top$, with $x_1 := y$,

$x_2 := \dot{y}$. In addition, $\bar{a}_i = [a_{i,1}, \ldots, a_{i,n}]$ and

$$X(x(k,t)) = R(x_1(k,t)) \begin{bmatrix} M_{C,1}\tilde{x}_1(k,t) \\ \vdots \\ M_{C,l}\tilde{x}_l(k,t) \end{bmatrix} - G(x_1(k,t)) - C(x_1(k,t), x_2(k,t)) - K(x_1(k,t), x_2(k,t)).$$

State-space system (4) is then discretised to give

$$\begin{aligned} x(k,t+1) &= f(x(k,t), u(k,t)), \qquad x(k,0) = x_0, \\ y(k,t) &= h(x(k,t)), \qquad t = 0,1,...,N-1. \end{aligned} \tag{6}$$

2.2 ILC Background

Since stroke rehabilitation requires repeated movements, ILC is a natural choice and has been used successfully in five clinical trials (focusing on elbow and shoulder motion) (Freeman, 2016). ILC is designed to be applied to tasks carried out repeatedly, and uses error information from each previous iterations to successively improve tracking performance.

To apply ILC, the system dynamics are efficiently packaged using the 'lifted' supervector notation[1]

$$u(k) = [u(k,0)^\top, u(k,1)^\top, ..., u(k,N-1)^\top]^\top, \tag{7}$$

$$y(k) = [y(k,1)^\top, y(k,2)^\top, ..., y(k,N)^\top]^\top, \tag{8}$$

$$y_d = [y_d(1)^\top, y_d(2)^\top, ..., y_d(N)^\top]^\top, \tag{9}$$

so that dynamics (6) can be equivalently written as

$$y(k) = g(u(k)), \text{ such that} \tag{10}$$

$$g(u(k)) = [g_1(u(k))^\top, ..., g_N(u(k))^\top]^\top, \tag{11}$$

with elements $i = 1,2,...,N$ given by

$$\begin{aligned} &g_i(x(k,0), u(k,0), ..., u(k,i-1)) \\ &\quad = h(f(f(...f(f(x(k,0), u(k,0)), u(k,1)), ... \\ &\qquad ..., u(k,i-2)), u(k,i-1)))). \end{aligned} \tag{12}$$

The most common form of ILC update is

$$u(k+1) = u(k) + Le(k), \tag{13}$$

in which $e(k) = y_d - y(k)$ and $L \in \mathbb{R}^{nN \times qN}$ is a suitable learning operator. For linear systems there are numerous options to design L to balance convergence and robustness, and these have been extended to the non-linear case by linearising the system between each trial about its current operating point (Freeman, 2014; Lin et al., 2006). For example, when applied to gradient-based ILC, the learning operator is given by

$$L = \gamma(g'(u(k)))^\top, \tag{14}$$

[1]The two-argument form $u(k,t)$ will be used to denote the along-the-trial form of a signal, with a single argument denoting the lifted form.

where $g'(u(k))$ is the Jacobian of $g(u(k))$, given by

$$g'(u(k)) := \left.\frac{\partial g(u)}{\partial u}\right|_{u=u(k)} = \begin{bmatrix} \frac{\partial g_1(u)}{\partial u(k)_1} & \cdots & \frac{\partial g_1(u)}{\partial u(k)_n} \\ \vdots & \ddots & \vdots \\ \frac{\partial g_q(u)}{\partial u(k)_1} & \vdots & \frac{\partial g_q(u)}{\partial u(k)_n} \end{bmatrix}. \tag{15}$$

2.3 Robust Stability of Standard ILC

Identifying $g(u(k))$ is exceptionally challenging due to the complexity of the human hand, which is sensitive to minor changes in electrode position and physiology. It also varies significantly between individuals, and over time due to fatigue. The approach used by (Freeman, 2014) was to identify $g'(u(k))$ between each iteration by carrying out an identification test on the patient, however this took over 10 minutes to track a single reference movement, making it unsuitable for practical use. One possible solution is to design L to maximise robustness, potentially using a single nominal model. The remainder of this section demonstrates the limitations of such an approach.

Define G^* as a lifted operator representing the true plant with the general dynamic form (10). Define C as the lifted operator corresponding to ILC scheme (13). These are configured as shown in Figure 2, where the signals have been renamed to account for the external disturbances $(u_0(k), y_0(k))^\top$. Hence $(u_1(k), y_1(k))$ denote the plant input and output, and $(u_2(k), y_2(k))^\top$ the ILC update and measured error signals. The operators can then be defined as

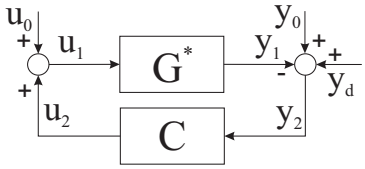

Figure 2: True plant and ILC feedback configuration.

$$G^* \quad : \quad u_1 \to y_2, \quad y_1(k) = g(u_1(k)), \tag{16}$$

and

$$C \quad : \quad y_2 \to u_2, \quad u_2(k+1) = u_2(k) + L_k y_2(k). \tag{17}$$

Since the true plant is unknown, the designer only has access to a non-linear model $g_p(u(k))$, giving

$$G_p \quad : \quad u_1 \to y_1, \quad y_1(k) = g_p(u_1(k)), \tag{18}$$

which is used to design a stabilising ILC law

$$C_p \quad : \quad y_2 \to u_2, \quad u_2(k+1) = u_2(k) + L_{k,p} y_2(k), \tag{19}$$

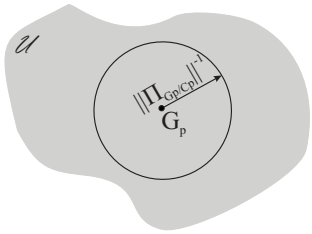

Figure 3: Uncertainty space showing stability region using a single ILC update designed for model G_p

where $L_{k,p}$ is designed based on the linearisation (15) of the model G_p.

The difference between plant model G_p and the true system G^* can be captured by the well-known gap metric, denoted $\delta(G_p, G^*)$, which is a bound on a mapping between their graphs. Using this metric, the following theorem lays out the conditions under which C_p is able to stabilise the true plant G^*.

Theorem 1. *Let ILC update C_p be designed such that the closed-loop system $[G_p, C_p]$ is gain stable, i.e. the map $\Pi_{G_p//C_p} : (u_0, y_0)^\top \to (u_1, y_1)^\top$ from external disturbances to internal signals has a finite bound. Then the true closed-loop system $[G^*, C_p]$ will be gain stable if the model mismatch satisfies*

$$\delta(G_p, G^*) < \|\Pi_{G_p//C_p}\|^{-1}. \tag{20}$$

Furthermore, the gap can be directly related to the underlying vector function forms as

$$\delta(G_p, G^*) \leq sup_{\|u\|\neq 0} \frac{\|g_p(u) - g^*(u)\|}{\|u\|}, \tag{21}$$

and if ILC is designed based on the sequence of linearised models $\{g'_p(u(k))\}_{k\in\mathbb{N}}$, this equates to

$$\delta(G_p, G^*) \leq sup_{k\in\mathbb{N},\, \|u\|\neq 0} \frac{\|(g'_p(u(k)) - g^*|_{u(k)})u\|}{\|u\|},$$

where $g^*|_{u(k)}\, u := g^*(u + u(k)) - g^*(u(k))$.

Proof. Adapted from (Georgiou and Smith, 1997) □

This states that ILC stabilises a 'ball' of plants with radius $\|\Pi_{G_p//C_p}\|^{-1}$ centred around G_p, as shown in Figure 3. However, if the model mismatch is too large, this region may not include G^* and $[G^*, C_p]$ will be unstable. This motivates multiple-model ILC, in which extra models and corresponding controllers are added to stabilise any possible true plant.

3 EMMILC STRUCTURE

EMMILC builds on the more general multiple model switched adaptive control (MMSAC) framework (Buchstaller and French, 2016). This section extends it for application to nonlinear systems. The idea of EMMILC is to design a set of plant models $\mathcal{G} = \{G_1, ..., G_m\}$ with associated ILC controllers $\mathcal{C} = \{C_1, ..., C_m\}$ such that a plant located anywhere within a user-defined uncertainty space $\mathcal{U}$ will be stabilised by one of these controllers. Switching between controllers is determined using a bank of estimators, $X_1, ..., X_m$, which compute a residual for each plant model. Each residual measures how closely a particular model matches the measured signals (u_2, y_2), and the model with smallest residual is switched into closed-loop. Figure 4 shows the overall structure.

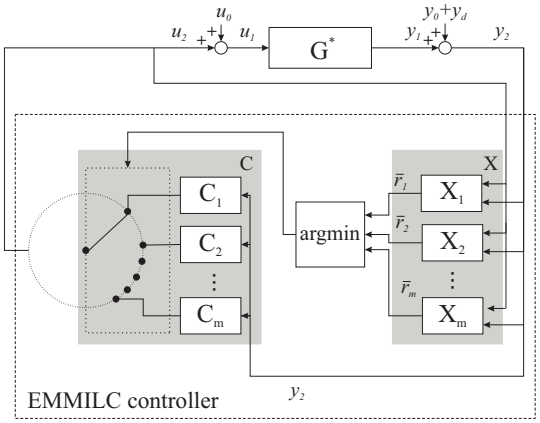

Figure 4: EMMILC block diagram

Based on the underlying theory in (Freeman and French, 2015), there are two conditions that must be satisfied to guarantee overall stability:

$$\text{(i)} \quad \exists\, G_i \in \mathcal{G}, \quad s.t. \quad \delta(G_i, G^*) < \rho(\mathcal{G}, \mathcal{C}, \mathcal{U}). \tag{22}$$

$$\text{(ii)} \quad \exists\, C_i \in \mathcal{C}, \quad s.t. \quad \|\Pi_{G//C_i}\| < \infty \quad \forall G \in \mathcal{U}. \tag{23}$$

where $\rho(\cdot)$ is defined in (Freeman and French, 2015). These ensure that the models $\{G_1, ..., G_m\}$ are sufficiently close together, and that there exists a controller within the set $\mathcal{C}$ able to stabilise all plants within the uncertainty space, as illustrated in Figure 5.

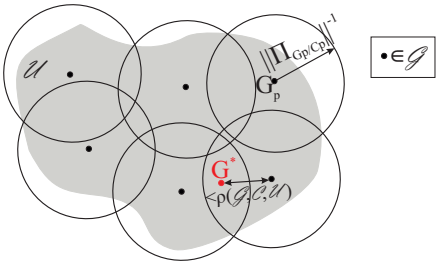

Figure 5: Model set requirements (22) and (23)

3.1 Estimator design

Estimator $X_p : (u_2, y_2)^\top \to r_p$ computes the smallest disturbance estimate (u_0, y_0) needed to explain the

observed signals (u_2, y_2) under the assumption that model G_p is the true plant. Let $\mathcal{N}_{p,k}^{[a,b]}(u_2, y_2)$ be the set of all possible disturbances compatible with G_p and observed signals $(u_2(k), y_2(k))$ over iterations $a, a+1, \ldots, b$. Then the residual is computed as

$$r_p(k) := \inf_{w_0} \{ r \geq 0 \mid r = \|w_0\|,\ w_0 \in \mathcal{N}_{p,k}^{[0,k]}(u_2, y_2) \} \tag{24}$$

The next theorem shows how this can be computed recursively, and provides a computationally tractable upper bound which can replace $r_p(k)$.

Theorem 2. *Residual computation (24) can be solved recursively using*

$$r_p(k) = \|r_p(k-1), i_p(k)\|, \quad r_p(0) = 0, \tag{25}$$

where the residual calculation for only iteration k is

$$i_p(k) = \inf_{w_0} \{ r \geq 0 \mid r = \|w_0\|,\ w_0 \in \mathcal{N}_{p,k}^{[k,k]}(u_2, y_2) \} \tag{26}$$

Furthermore, $i_p(k)$ has the upper bound

$$\|y_2(k) - g_p(u_2(k))\| \tag{27}$$

so that an upper bound, $\tilde{r}_p(k)$, can be computed as

$$\tilde{r}_p(k) = \sqrt{\sum_{i=0}^{k} \|y_2(i) - g_p(u_2(i))\|^2} \tag{28}$$

Proof. Relations (25), (26) follows from the l_2 identify $\|\|x\|, \|y\|\| = \|(x, y)\|$ for $x, y \in l_2$, and the fact that the dynamics of one ILC trial do not affect the next. From Fig. 4, the signals compatible with G_p satisfy $y_2(k) = g_p(u_2(k) + u_0(k)) + y_0(k)$. An upper bound on (26) is achieved by setting $u_0 = 0$ to obtain

$$\begin{aligned} i_p(k) &\leq \inf_{y_0, u_0 = 0} \{ r \geq 0 \mid r = \|w_0\|,\ w_0 \in \mathcal{N}_{p,k}^{[k,k]}(u_2, y_2) \} \\ &= \inf_{y_0, u_0 = 0} \{ r \geq 0 \mid r = \left\| \begin{pmatrix} u_0(k) \\ y_0(k) \end{pmatrix} \right\|, \\ &\qquad\qquad y_0 = y_2(k) - g_p(u_2(k) + u_0(k)) \}, \\ &= \|y_2(k) - g_p(u_2(k))\| \end{aligned} \tag{29}$$

and (28) follows by combining (29) and (25). □

Remark 1. *Lifted residual calculation (28) can be modified to account for parameter variation, e.g. due to muscle fatigue, by introducing a discount factor $0 \leq \lambda < 1$ such that*

$$\tilde{r}_p(k) = \sqrt{\sum_{i=1}^{k} \lambda^{k-i} \|y_2(i) - g_p(u_2(i))\|^2} \tag{30}$$

4 FRAMEWORK APPLICATION

EMMILC is now applied to FES array motion control.

4.1 EMMILC design procedure

The following steps outline the practical implementation of the EMMILC framework.

1. **Model structure:** Establish a suitable parameterised form to capture the true plant $g^*(u)$.
2. **Uncertainty space $\mathcal{U}$:** Identify the range in model parameters necessary to capture the variation in the true dynamics. The set union is $\mathcal{U}$.
3. **Controller design procedure:** Formulate an ILC design procedure $K : G_p \to C_p$ that stabilises the closed-loop $[G_p, C_p]$. This will balance convergence with robustness, as measured by (20).
4. **Model set $\mathcal{G}$:** Construct a model set $\mathcal{G}$ with corresponding controller set $\mathcal{C}$ to give sufficient coverage of the uncertainty space. Criteria (22) and (23) can be combined into a single condition
$$\forall\, G_i,\ \exists G_j \in \mathcal{G},\ G_i \neq G_j,\ s.t.\ \delta(G_i, G_j) < \Delta, \tag{31}$$
where parameter Δ defines the maximum distance between neighbouring models. Smaller values will improve the likelihood of a stable design but will have a higher computational cost.
5. **Estimator set:** For each model, implement estimator X_p using (30). Tune λ to balance sensitivity against adaptability to changing dynamics.

The following subsections apply this design framework using the model form introduced in Section 2.1.

4.2 Specific Model Structure

The human hand and wrist contains 15 joints actuated by over 20 muscles, however 42% of functional movements involve only four fingers moving in unison (Ingram et al., 2008). Furthermore, the spasticity commonly experienced by stroke patients makes the extensor muscles a critical target for rehabilitation (American Stroke Association, 2022). Therefore, the model used in this work contains $l = 4$ extrinsic muscles of the hand, namely the extensor communis (EC), Extensor carpi radialis brevis (ECRB), Extensor indicis (EI), and Extensor carpi ulnaris (ECU). The wrist and metacarpophalangeal (MCP) joints were actively controlled, and are defined in Figure 6, resulting in the output vector $y(k,t) = [\theta_1(k,t), \theta_2(k,t)]^\top$.

Stimulation was applied using a 4×6 element electrode array (such as that used in (Freeman et al., 2016)), giving a total of 24 elements. Preliminary experiments revealed that all four muscles of interest could be activated using only two electrode elements. The optimal location of these was determined heuristically for each participant, and the pulse-width

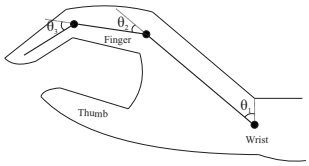

Figure 6: Joint angle definitions

applied to these elements was used as the input to the system, giving $n = q = 2$.

The IRC form was chosen as

$$z_i = a_1 \frac{e^{a_2 v_i} - 1}{e^{a_2 v_i} + a_3}. \tag{32}$$

which has been been shown to accurately capture muscle dynamics using only a small number of parameters a_1-a_3 (Freeman et al., 2009). Similarly, the LAD were modelled as a second order, critically damped system with natural frequency ω_n.

The forms of $M(y)$, $C(y,\dot{y})$, and $R(y)$ were equivalent to those given in (Theodorou et al., 2011), whilst gravity was integrated within $K(y,\dot{y})$. This then assumed a simple linear friction form, in which each joint is represented as a spring with stiffness k_i, damping b_i, and zero elongation at the initial position $\theta_{0,i}$:

$$K(y,\dot{y}) = \begin{bmatrix} k_1(\theta_{0,1} - \theta_1) + b_1\dot{\theta}_1 \\ \vdots \\ k_q(\theta_{0,q} - \theta_q) + b_q\dot{\theta}_q \end{bmatrix}. \tag{33}$$

The physiological constraints of the joint were modelled by increasing joint stiffness k as the angle θ approaches a cutoff value θ_{cutoff}. This is expressed by

$$k_i(\theta_i) = \frac{0.1k_{n,i}(\theta_{thres,i} - \theta_{cutoff,i})}{\theta_i - \theta_{cutoff,i}} + k_{n,i},\ i = 1,\ldots,q \tag{34}$$

where $k_{n,i}$ is the nominal joint stiffness of joint i, and $\theta_{thres,i}$ the threshold angle at which the stiffness begins to increase. Implementation was simplified by selecting a large value of T_s and setting $N = 1$. In this context the output $y(k)$ represents the steady-state response to input $u(k)$. This approach has been used previously in (Sun and Freeman, 2024), and is applicable to the FES rehabilitation setting, in which dynamics are slow and the overall shape of the trajectory is more important than the movement speed.

4.3 EMMILC Design

After establishing the model structure, the next step is to define the uncertainty space $\mathcal{U}$. Preliminary experiments revealed that parameters k_i, $\theta_{0,i}$, and $\theta_{cutoff,i}$, $i = \{1,2\}$ had the most impact on model performance, however, $\theta_{0,i}$ and $\theta_{cutoff,i}$ could be easily measured experimentally (see Section 5). The joint stiffness k_1 and k_2 were therefore selected to define the uncertainty space, with bounds $k_1, k_2 \in [0.2, 2]$ corresponding to the range of values measured in (Park et al., 2017). Preliminary experiments revealed that this was a sufficient range to cover possible parameter variation.

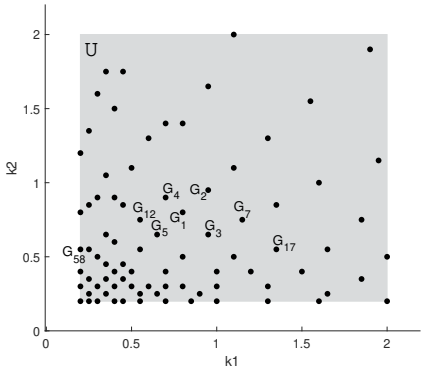

Figure 7: Model set distribution, with key models labelled

The control design procedure K was selected as linearisation-based gradient ILC, as given by (13), (14), due to its favourable robustness properties.

Preliminary tests were carried out in which EMMILC design parameters were tuned heuristically to give optimal values of $\gamma = 10{,}000$, $\Delta = 0.0007$, and $\lambda = 0.4$. Parameter γ was selected to ensure robust convergence within 15 iterations, whilst Δ was selected as a trade-off between minimising computation time (mean of 3.7s per trial) and ensuring stability. The resulting model set distribution is shown in Figure 7. The low λ value allowed the system to quickly adapt to unforeseen changes in system dynamics.

5 EXPERIMENTAL TESTING

Extensive simulation was first undertaken using in-silico data to demonstrate system feasibility. Results are omitted for brevity but can be found online at https://doi.org/10.5258/SOTON/D3186. Experimental tests were then carried out on four unimpaired participants, following ethical approval from the University of Southampton (ERGO: FEPS 91636).

5.1 Method

Code was written in Matlab 2024a and deployed in realtime onto a Raspberry Pi 3B. This provided PWM outputs that were amplified using a 4-channel stimulator (Odstock Medical Ltd, Salisbury UK), whilst joint angles were recorded using a contactless motion-capture sensor (Ultraleap Stereo IR 170). The setup

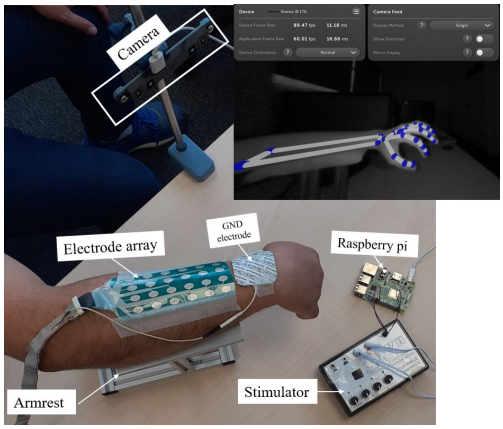

Figure 8: Experimental setup showing motion tracking

Table 1: EMMILC and ID-based ILC performance

Participant		y_d	Error norm	k^*
1	ID-based	[65.4,-9.8]	0.1065	13
	EMMILC		0.0236	4
2	ID-based	[79.9, -9.3]	0.3958	>24
	EMMILC		0.1801	4
3	ID-based	[80.2,-20.0]	0.2727	10
	EMMILC		0.2304	2
4	ID-based	[57.5, -7.7]	1.372	19
	EMMILC		0.3141	2

is shown in Figure 8.

For each participant a feasible reference was first determined, as given in Table 1, corresponding to a pointing posture. The values of θ_0 were recorded as the resting joint angles, before the maximum stimulation pulsewidth ($300\mu s$, in accordance with FES safety protocols) was applied to both channels, with the resulting angles giving θ_{cutoff}. These values were then used to define the model.

The performance of EMMILC was compared to the best existing electrode array control approach, in which the ILC algorithm employs a linearised model that is identified between trials using tests on the physical patient (Sun and Freeman, 2024). Each iteration of identification-based (ID-based) ILC requires $n+1$ tests (1 ILC update and n identification tests).

5.2 Results

Table 1 compares the performance of EMMILC to that of ID-based ILC, in terms of the error norm after 15 tests, defined by

$$\text{Error norm} = \|y_d - y(15)\|_2, \tag{35}$$

and the number of iterations (denoted k^*) required for the error to converge to 30% of its initial value.

This reveals that the average error norm over all participants after 15 iterations is 65% lower when using EMMILC as compared with ID-based ILC, requiring on average 13 fewer tests to converge.

Figure 9a gives an example of the convergence of EMMILC and ID-based ILC for one participant, demonstrating that EMMILC convergence requires significantly fewer tests. EMMILC switching is shown in Figure 9b, which reveals that the algorithm quickly switches to a stabilising model and stays there for the remaining trials. The key models that the system switches to are shown in Figure 7.

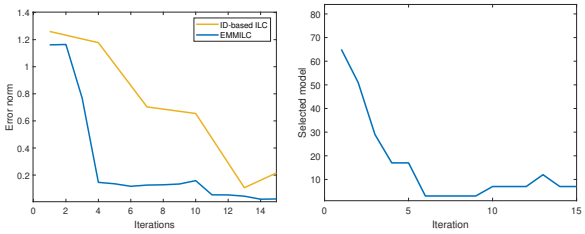

(a) Error convergence (b) EMMILC switching

Figure 9: Example performance for participant 1

6 CONCLUSIONS AND FUTURE WORK

This paper has presented a novel approach to the control of electrode arrays using multiple-model iterative learning control. It first extended EMMILC for application to nonlinear systems, and then developed a transparent framework for the design of a suitable model-set, estimator, and controller. It then demonstrated the effectiveness of EMMILC in experiments with unimpaired participants. These revealed that it could reduce the average number of tests for convergence by 13 compared to standard identification-based ILC algorithms.

Areas for future work include carrying out experimental tests on stroke patients, increasing the number of inputs in order to activate a carefully-chosen subset of electrodes, and improving EMMILC performance by increasing the dimension of the uncertainty space.

REFERENCES

American Stroke Association (2022). Lets talk about spasticity after stroke.

Brend, O., Freeman, C., and French, M. (2015). Multiple-model adaptive control of functional electrical stimulation. *IEEE Transactions on Control Systems Technology*, 23(5):1901–1913.

Buchstaller, D. and French, M. (2016). Robust stability for multiple model adaptive control: Part ithe framework. *IEEE Transactions on Automatic Control*, 61(3):677–692.

Feigin, V. L., Brainin, M., Norrving, B., Martins, S., Sacco, R. L., Hacke, W., Fisher, M., Pandian, J., and Lindsay, P. (2022). World stroke organization (wso): Global stroke fact sheet 2022. *International journal of stroke*.

Feldman, A. G. and Latash, M. (2005). Testing hypotheses and the advancement of science: recent attempts to falsify the equilibrium point hypothesis. *Brain Res*, 145(91103).

Freeman, C. and French, M. (2015). Estimation based multiple model iterative learning control. In *2015 54th IEEE Conference on Decision and Control (CDC)*, pages 6070–6075.

Freeman, C., Hughes, A.-M., Burridge, J., Chappell, P., Lewin, P., and Rogers, E. (2009). A model of the upper extremity using fes for stroke rehabilitation. *Journal of biomechanical engineering*, 131:031011.

Freeman, C., Yang, K., Tudor, J., and Kutlu, M. (2016). Feedback control of electrical stimulation electrode arrays. *Medical Engineering and Physics*, 38(11):11851194.

Freeman, C. T. (2014). Electrode array-based electrical stimulation using ILC with restricted input subspace. *Control Engineering Practice*, 23:3243.

Freeman, C. T. (2016). *Control System Design for Electrical Stimulation in Upper Limb Rehabilitation*. Springer International Publishing. Springer International Publishing.

Georgiou, T. T. and Smith, M. C. (1997). Robustness analysis of nonlinear feedback systems: An inputoutput approach. *IEEE Transactions on Automatic Control*, 42(9):12001221.

Hebb, D. O. (1949). *Organization of Behavior*. Psychology Press.

Hughes, A.-M., Burridge, J., Demain, S., Ellis-Hill, C., Meagher, C., Tedesco Triccas, L., Turk, R., and Swain, I. (2014). Translation of evidence-based assistive technologies into stroke rehabilitation: Users' perceptions of the barriers and opportunities. *BMC health services research*, 14:124.

Ingram, J., Kording, K., Howard, I., and Wolpert, D. (2008). The statistics of natural hand movements. *Experimental brain research. Experimentelle Hirnforschung. Expérimentation cérébrale*, 188:223–36.

Kwakkel, G., Kollen, B. J., van der Grond, J., and Prevo, A. J. H. (2003). Probability of regaining dexterity in the flaccid upper limb: impact of severity of paresis and time since onset in acute stroke. *Stroke*, 34 9:2181–6.

Le, F., Markovsky, I., Freeman, C. T., and Rogers, E. (2010). Identification of electrically stimulated muscle models of stroke patients. *Control Engineering Practice*, 18(4):396–407.

Lin, T., Owens, D., and Hatonen, J. (2006). Newton method based iterative learning control for discrete non-linear systems. *International Journal of Control*, 79(10):12631276.

ODwyer, S., OKeeffe, D., Coote, S., and Lyons, G. (2006). An electrode configuration technique using an electrode matrix arrangement for fes-based upper arm rehabilitation systems. *Medical Engineering & Physics*, 28(2):166–176.

Park, K., Chang, P.-H., and Kang, S. H. (2017). In vivo estimation of human forearm and wrist dynamic properties. *IEEE Transactions on Neural Systems and Rehabilitation Engineering*, 25(5):436–446.

Persson, H. c., Parziali, M., Danielsson, A., and Sunnerhagen, K. (2012). Outcome and upper extremity function within 72 hours after first occasion of stroke in an unselected population at a stroke unit. a part of the salgot study. *BMC neurology*, 12:162.

Salchow, C., Valtin, M., Seel, T., and Schauer, T. (2016). A new semi-automatic approach to find suitable virtual electrodes in arrays using an interpolation strategy. *European Journal of Translational Myology*, 26(2).

Schill, O., Rupp, R., Pylatiuk, C., Schulz, S., and Reischl, M. (2009). Automatic adaptation of a self-adhesive multi-electrode array for active wrist joint stabilization in tetraplegic sci individuals. In *2009 IEEE Toronto International Conference Science and Technology for Humanity (TIC-STH)*, pages 708–713.

Stockley, R., Peel, R., Jarvis, K., and Connell, L. (2019). Current therapy for the upper limb after stroke: a cross-sectional survey of uk therapists. *BMJ Open*, 9(9).

Sun, X. and Freeman, C. T. (2024). Parameterised function ILC with application to stroke rehabilitation. *Control Engineering Practice*, 145.

Theodorou, E., Todorov, E., and Valero-Cuevas, F. J. (2011). Neuromuscular stochastic optimal control of a tendon driven index finger model. In *Proceedings of the 2011 American Control Conference*, page 348355. IEEE.